A. Schneider[a], C. Stallybrass[a], J. Konrad[a], A. Kulgemeyer[a], H. Meuser[b], S. Meimeth[b]
[a] Salzgitter Mannesmann Forschung GmbH, Duisburg, Germany
[b] Mannesmannröhren Mülheim GmbH, Mülheim an der Ruhr, Germany

Formation of primary TiN precipitates during solidification of microalloyed steels – Scheil versus DICTRA simulations

Modern high-strength low-alloy steels commonly contain microalloying additions of titanium, niobium or vanadium in different combinations in order to obtain the desired microstructure and mechanical properties. Titanium has a strong tendency to form TiN in the range of the solidus temperature. This has been reported to have a negative effect on the impact toughness of the material. Thermodynamic calculations showed that the titanium and nitrogen content and the titanium to nitrogen ratio determine if the formation of TiN takes place during solidification or in the solid state. These calculations where complemented by simulations of solidification using the Scheil–Gulliver model and DICTRA. The results were compared with microstructure investigations of plate and slab material with titanium contents between 0.003 wt.% and 0.015 wt.% using light-optical microscopy and electron probe microanalysis. While the formation of TiN particles cannot be ruled out even at the lowest Ti levels, the temperature of formation and the volume fraction varied significantly depending on the Ti content. With respect to the first results of this preliminary study, i.e. the comparison of equilibrium, Scheil and DICTRA calculations, it can be assumed that the Scheil model is the most appropriate one at present.

Keywords: Micro-alloyed steels; TiN; Solidification; DICTRA; Scheil–Gulliver model

1. Introduction

Modern high strength low-alloy steels commonly contain microalloying elements such as titanium, niobium or vanadium, which all play a major role in the evolution of the microstructure during thermomechanical rolling. These elements form carbonitrides at different temperatures depending on their respective solubility in the parent phase. Nitrogen-rich titanium carbonitrides are stable during reheating at temperatures in the range of 1200 °C and therefore prevent excessive grain coarsening if alloyed in the correct quantity [1]. Niobium, which has a higher solubility in the austenite than titanium, can be completely dissolved in the austenite during reheating and forms carbon-rich precipitates during thermomechanical rolling, which considerably retard recrystallisation of the austenite, leading to the desired fine-grain microstructure with high strength and excellent low temperature toughness [2].

It has been reported that coarse titanium carbonitrides that may form during solidification can have a negative effect on the toughness of the material [3]. The moment and the location of the precipitation of primary titanium carbonitrides within continuous cast slabs depend on the titanium content and on the processing conditions during continuous casting.

The aim of the present investigation was to study the formation of titanium carbonitrides during continuous casting using DICTRA, a software package for the simulation of diffusion controlled processes in multi component alloys, with basic assumptions with regard to cooling rate and to compare the results with those obtained with a Scheil–Gulliver model. The results of these theoretical investigations are then compared with the microstructure of continuous cast material with different titanium levels.

The long-term aim of this research and development project is to provide a predictive tool allowing an estimation of the tendency of primary TiN formation in microalloyed steels for pipeline production.

A typical chemical analysis of a microalloyed steel for pipeline production is as follows: Fe-0.04/0.09C-0.1/0.3Si-1.3/1.9Mn-Nb-Ti-N (wt.%). In this work the discussion of solidification and TiN precipitation is performed by means of quinary Fe–C–Nb–Ti–N model alloys: Fe-0.04C-0.04Nb-0.003/0.025Ti-0.002/0.005N. Finally an outlook towards more realistic alloy systems is given by the simulation result of a 9-component system.

It has to be mentioned that a direct correlation of experimental results on multi-component steels with the simulations on quinary model alloys is still an unsolved challenging task.

2. Experimental

The chemical composition of slab and plate samples being investigated by electron probe microanalysis (EPMA) varied as follows:

Fe-0.04C-0.3Si-1.3Mn-0.009P-0.0004S-0.01Mo-0.036Nb-0.003/0.014Ti-0.002/0.005N (wt.%).

The samples for the EPMA investigations were taken from slab material in the as-cast condition as well as from plate material after the thermomechanically controlled process (TMCP). Assuming no change in the segregation of substitution elements by diffusion during TMCP, the microstructure of the plate samples was expected to reveal a compressed segregation structure dependent on the deformation degree. The samples were taken as diagonal cross-sections inclined towards the casting or rolling direction, respectively. The purpose of this sampling was the geometrical expansion of the sampled area, thus increasing the spatial

resolution of the analysis. The samples had dimensions of $100 \times 100 \times 5$ mm^3.

All samples were investigated by means of area scans of the local content of Mn of the full samples surface (100×100 mm^2, 100 µm step size). The element distributions of selected samples were additionally analysed at higher resolution. Areas of 1×1 mm^2 were investigated with a step size of 2 µm recording the contents of Mn, Ti and N. The high resolution scans were intended particularly to detect large TiN precipitates within the segregation zones.

3. Thermodynamic calculations

In this work, three different methods of computational thermodynamics are applied to predict the solidification sequences of the microalloyed steels. The phase equilibria are calculated using the software Thermo-Calc with the thermodynamic database TCFE3 [4, 5].

Since equilibrium calculations do not reflect segregation of elements the Scheil solidification model was applied [6]. In this model a stepwise cooling is calculated by taking into account the continuously changing composition of the liquid. The Scheil solidification model assumes that solute diffusion in the solid phase is small enough to be considered negligible. Diffusion in the liquid is treated by defining extremely high mobilities of the species. The Scheil model in Thermo-Calc is implemented in a way that C and N can also be defined as fast diffusing species in the solid.

The transformation kinetics are simulated using the software DICTRA (calculation of DIffusion Controlled TRAnsformations) with the mobility database MOB2 [7, 8]. The diffusional processes are treated while taking the thermodynamics of the system fully into account. The solidification and solid–solid transformation simulations are treated by DICTRA on the basis of fundamental concepts as described in [7, 9–13]. For this work two main parameters, e. g. the cooling rate $\dot{T}$ and the secondary arm spacing λ_2 are defined without any experimental background. The cooling rate is assumed to be 0.2 K s^{-1} which is reasonably within a range being reported by Goto et al. [14]. Using a formula for a correlation between secondary arm spacing and cooling rate for low-alloyed steels λ_2 can be estimated to be ~ 270 µm [15]. For simplification of the simulations λ_2 was defined to be 200 µm. The solidification simulation using DICTRA is treated in a planar geometry by defining a cell of 100 µm in length representing half the secondary dendrite arm spacing of 200 µm. This cell contains the phases liquid, δ-ferrite, austenite (γ) and TiN as shown in Fig. 1.

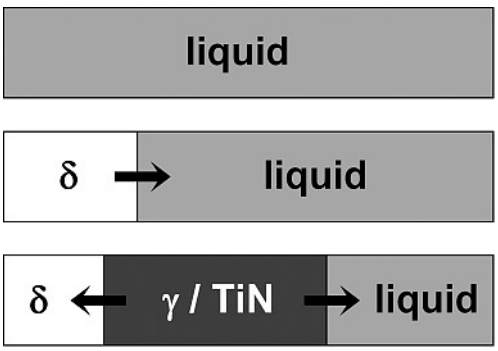

Fig. 1. DICTRA cell model for simulation of solidification.

4. Results

The chemical analysis of the alloy presented in Figs. 2 and 3 is Fe-0.04C-0.3Si-1.3Mn-0.009P-0.0004S-0.01Mo-0.036 Nb-0.010Ti-0.0028N (wt.%).

The Mn element map of the full sample scans in Fig. 2 shows the stretched segregation structure of the slab and the plate material of this alloy. The slab shows a significantly coarser structure than the plate due to the deformation of the latter. The analysed sample of the slab material does not show a strong segregation zone. This indicates that the macrosegregation is not homogeneously distributed with respect to casting and transverse direction. Within the plate sample, a pronounced deformed segregation zone with Mn contents of 1.66 % (compared to an average of 1.34 %) was observed. The position in the sample corresponds to the centre of the plate.

In the high resolution Mn and Ti element maps of the plate material acquired close to this segregation area (see

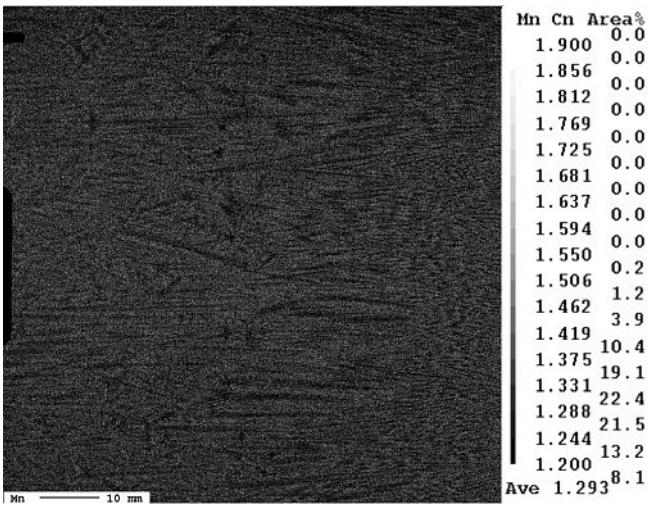

(a)

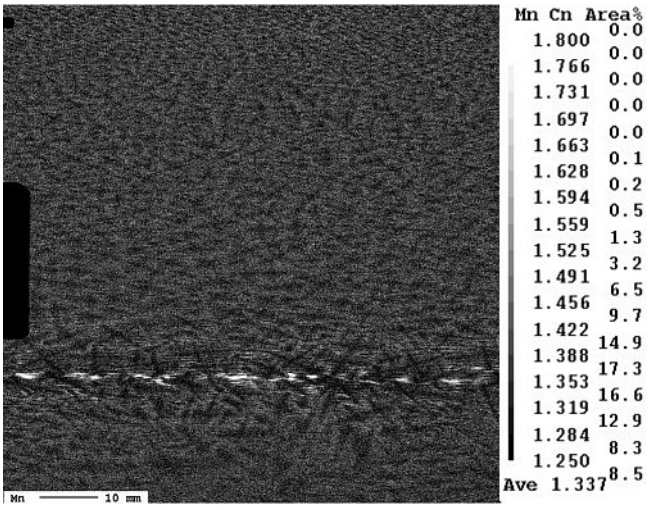

(b)

Fig. 2. Area analysis map of the Mn content acquired performing EPMA on 100×100 mm^2 diagonal cut samples of (a) of the continuously cast slab and (b) of the rolled sheet. A step width of 100 µm was used; black areas on the left are parts of the sample holder. The variation of the chemical composition is plotted on the right in weight percent.

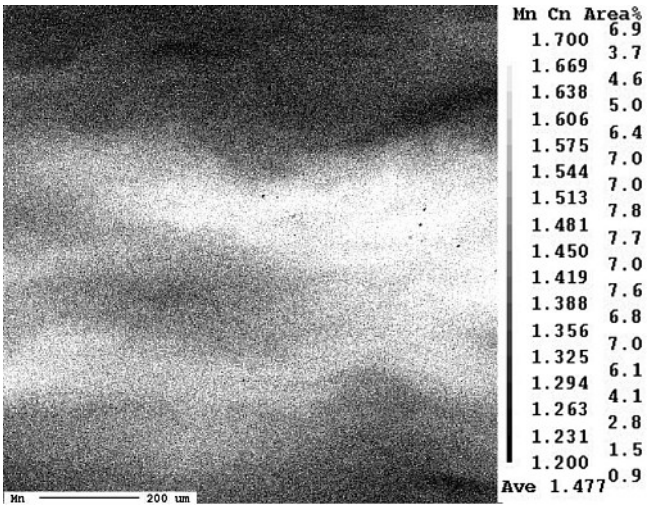

(a)

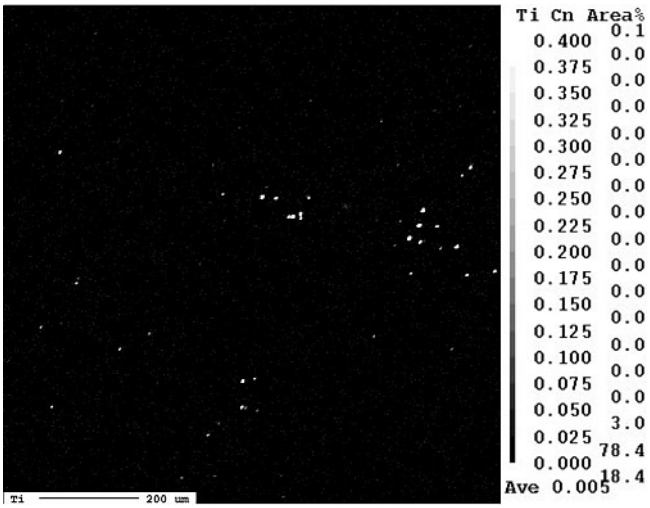

(b)

Fig. 3. Area analysis map of (a) the Mn and (b) the Ti content acquired performing EPMA on 1×1 mm^2 diagonal cut samples of the rolled sheet close to the sheet centre. A step width of 2 µm was used. The variation of the chemical composition is plotted on the right in weight percent.

Fig. 3), the maxima of the measured Mn content are even higher (up to 1.7 %). This effect is caused by the higher resolution. The interaction volume in which the analysed characteristic X-rays are generated at each measurement spot is reduced from 20 µm (100 µm step size) to 0.5 µm (2 µm step size). The probability of acquiring the X-ray intensity from an area of maximum Mn content is therefore increased.

The same effect holds for the Ti map. While the large step size would only allow for an indication of very large (>50 µm) Ti-rich particles, the high resolution measurement can already indicate one of a size larger than 0.5 µm. The particle size cannot be estimated by the performed EPMA mappings because the measurement spot generates an integral element content value dependent on the position – matrix or particle.

The large TiN precipitates expected in the investigated alloys were successfully detected applying the method described. In particular, the high number of such TiN precipitates in the macrosegregation zones in contrast to the low

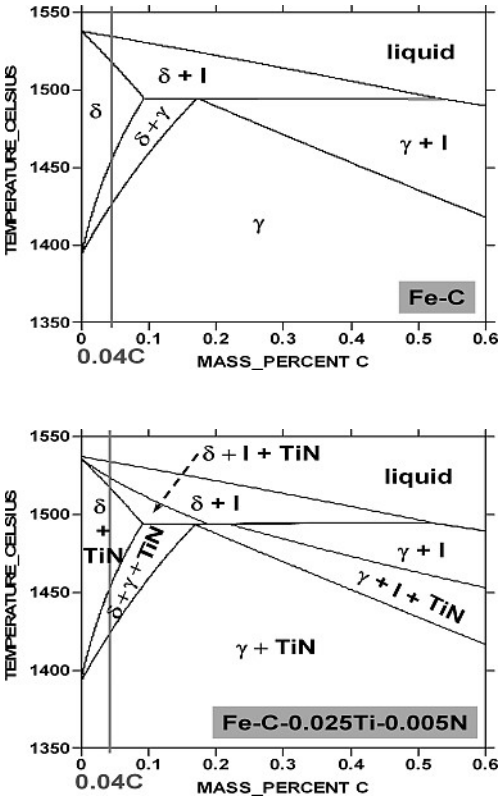

Fig. 4. Fe–C phase diagram (upper diagram) and isopleth of Fe–C-0.025Ti-0.005N (lower diagram).

numbers in other areas was significant. Furthermore, it could be shown that large TiN precipitates are also present in samples of alloys with low Ti levels at which the equilibrium calculations via Thermo-Calc did not predict their existence.

The high-temperature part of the binary Fe–C phase diagram is shown in Fig. 4 (upper part). The lower part of Fig. 4 shows the influence of adding 0.025 wt.% Ti and 0.005 wt.% N on the phase equilibria. The formation of TiN in the liquid can be expected even for equilibrium conditions (see vertical section line at 0.04 wt.% C).

In Fig. 5 an example of phase equilibria in a quinary alloy with 0.04 wt.% Nb is shown. When comparing this diagram with Fig. 4 (lower part) it can be seen that the lower titanium and nitrogen contents result in a stability range to TiN clearly below the solidus temperature. The Scheil calculation of the solidification sequences of the same alloy indicates a tendency to TiN precipitation within the melt.

Equilibrium and Scheil calculations were performed for all five model alloys as summarised in Table 1. Considering phase equilibria within the relatively unsystematic choice of alloy compositions an amount of 0.010 wt.% Ti and 0.028 wt.% N is required for TiN formation in the liquid. In contrast, the Scheil calculations indicate TiN formation already for low Ti (0.003 wt.%), but relatively high N (0.005 wt.%) contents.

The same alloy compositions were used in the DICTRA simulations of the solidification kinetics.

Figures 6 and 7 represent the DICTRA results for the alloy Fe-0.04C-0.04Nb-0.025Ti-0.002N. The diagram in Fig. 6 shows the temperature versus fraction of solid which can also be calculated by the Scheil model. Comparisons of

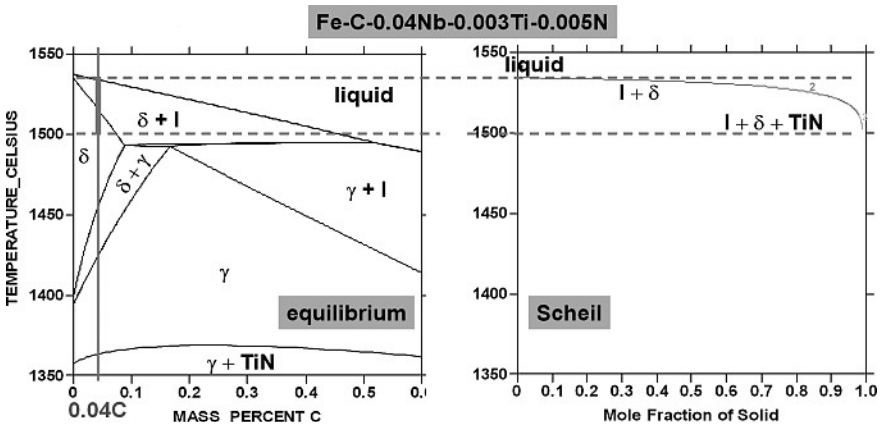

Fig. 5. Isopleth of Fe–C-0.04Nb-0.003Ti-0.005N (left) and corresponding Scheil calculation for Fe-0.04C-0.04Nb-0.003Ti-0.005N (right).

Table 1. Comparison of solidification sequences as calculated by Thermo-Calc (equilibrium and Scheil) and DICTRA for the various quinary model alloys.

chemical composition	solidification sequence		
Fe-0.04C-0.04Nb-	Equilibrium	Scheil fast diffusing C and N	DICTRA cooling rate: 0.2 K s^{-1}
-0.003Ti-0.002N	L → L + δ → δ	L → L + δ → δ	L → L + δ → δ
-0.003Ti-0.005N	L → L + δ → δ	L → L + δ → L + δ + TiN → δ + TiN	L → L + δ → δ
-0.010Ti-0.0028N	L → L + δ → L + δ + TiN → δ + TiN	L → L + δ → L + δ + TiN → δ + TiN	L → L + δ → δ
-0.012Ti-0.002N	L → L + δ → δ	L → L + δ → L + δ + TiN → δ + TiN	L → L + δ → δ
-0.025Ti-0.002N	L → L + δ → δ	L → L + δ → L + δ + TiN → δ + TiN	L → L + δ → L + δ + TiN
-0.025Ti-0.005N	L → L + δ → L + δ + TiN → δ + TiN	L → L + δ → L + δ + TiN → δ + TiN	L → L + δ → L + δ + TiN

such diagrams generated by both Thermo-Calc, Scheil and DICTRA calculations help to predict general tendencies such as TiN formation in the liquid. The more detailed diagram in Fig. 7 shows concentration profiles of elements versus distance (half a secondary dendrite arm spacing) for different time periods. It can be clearly seen that N is homogeneously distributed in the solid for all time steps owing to fast diffusion. In the case of Ti, diffusion takes place by forming concentration profiles with increasing Ti contents with increasing time. The flattening of the microsegregation profiles by diffusion in the solidified material during cooling is not studied in this work.

In the case of TiN formation in the liquid (Fe-0.04C-0.04Nb-0.025Ti-0.002/0.005N, see Table 1) the DICTRA simulation is not continued after onset of TiN growth. In the other cases the diffusional processes in the δ-ferrite are calculated during cooling down to around 1470 °C.

In order to define more realistic simulations of solidification processes it is necessary to include more elements. In Fig. 8 an example of a solidification simulation of a multi-component system Fe–C–Si–Mn–P–Mo–Nb–Ti–N is shown. The microsegregation profiles of Mn and P are plotted for different time steps.

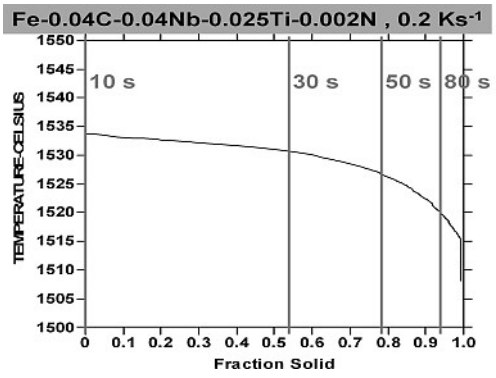

Fig. 6. Result of solidification simulation using DICTRA of a Fe-0.04C-0.04Nb-0.025Ti-0.002N model alloy. The result is plotted as temperature versus fraction of solid, as is usually done for the Scheil calculations.

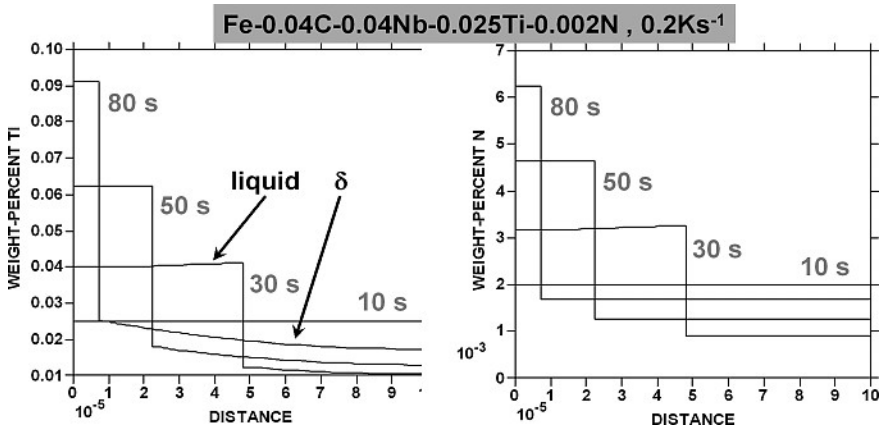

Fig. 7. Solidification simulation using DICTRA of a Fe-0.04C-0.04Nb-0.025Ti-0.002N model alloy: Ti and N composition profiles for the time steps 10, 30, 50, and 80 s.

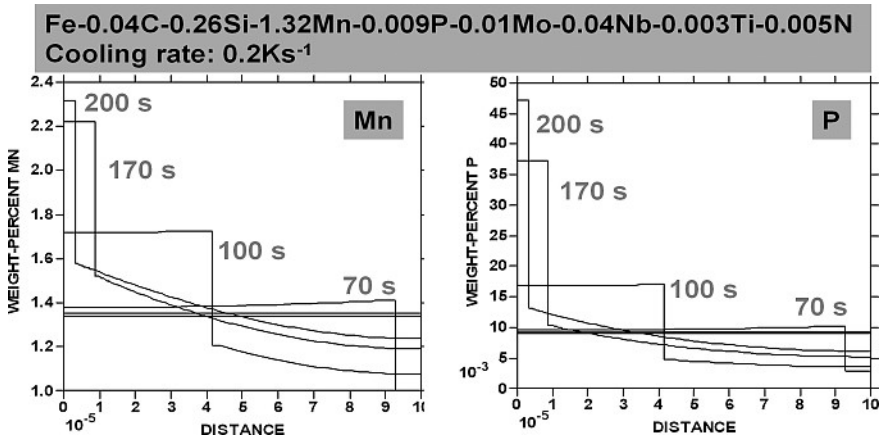

Fig. 8. Solidification simulation using DICTRA of a Fe-0.04C-0.26Si-1.32Mn-0.009P-0.01Mo-0.04Nb-0.003Ti-0.005N model alloy: Mn and P composition profiles for the time steps 30, 60, 70, 100, 170, and 200 s.

The DICTRA simulations shown above were performed for nominal global compositions. The microsegregation of the elements can be directly plotted as composition profiles versus distance representing half a secondary arm spacing (see Figs. 7 and 8). The macrosegregation is a combined result of microsegregation and also transport phenomena in continuous casting of the steels. Although the EPMA analysis revealed the presence of large TiN particles in the centreline segregation of an Fe-0.04C-0.3Si-1.3Mn-0.009P-0.0004S-0.01Mo-0.036Nb-0.010Ti-0.0028N alloy (see Fig. 3) the DICTRA simulation did not give any indication of their appearance (see Table 1). Therefore, it was decided to use the microanalysis (EPMA) results of the centreline segregation for defining another chemical composition including another element, i. e. Mn, with a significantly higher content (1.6 instead of 1.3 wt.%). The simulation result again does not show any tendency toTiN formation in the liquid, not even for an assumed fairly large Mn content of 1.9 wt.%. The EPMA mappings of the macrosegregation area did not reveal any significant Ti enrichment within the given measurement accuracy.

5. Discussion and conclusions

The EPMA measurements on the real multi-component slab and plate material cannot directly be correlated to the results of the computational thermodynamics calculations. Although this fact can be regarded as a drawback of this work it should be emphasised that exactly the detection of Ti enrichments (leading to the conclusion of the existence of relatively large TiN precipitates) has initiated more sophisticated calculations leading to more realistic results than pure equilibrium calculations. As described above the solidification simulations using DICTRA were performed on the basis of assuming a certain secondary dendrite arm spacing and a cooling rate. These parameters are of course dependent on time and on the location in the slab. These aspects are not taken into account in this study. Therefore, it cannot be excluded that a variation in the cooling rate, for instance, would change the solidification conditions in a way that TiN formation in the liquid would also be possible for Fe-0.04C-0.036Nb-0.010Ti-0.0028N as indicated by both equilibrium and Scheil calculations.

With respect to the poor knowledge of the solidification parameters, especially the unknown local distribution of the cooling rate within the slab, no real conclusion can be drawn concerning the choice of the prediction method.

Additionally, the mobilities of the alloying elements should also be taken into account with respect to the numerical treatment of diffusional processes during cooling. This will be performed in an ongoing study focussing on more experimental investigations combined with computational thermodynamics. Within this study microprobe investigations will be performed on micro- and macrosegregation areas taking into account all relevant alloying elements in order to find a better correlation between segregation and TiN formation. However, as a first approach this work can serve as a pre-study for a treatment of these complex processes.

With respect to the first results of this study, i. e. the comparison of equilibrium, Scheil and DICTRA calculations, it can be assumed that the Scheil model is the most appropriate one at present (see Table 1).

In a further study, a complete comparison of experimentally detected and calculated segregation profiles should be performed that takes all relevant elements such as Fe, C, Si, Mn, P, S, Mo, Nb, Ti, and N into account. Also, the cooling rate and the secondary arm spacing should be systematically varied and compared to experimental results (e. g. EPMA measurements of the microsegregation profiles). Since DICTRA simulations are based on a one-dimensional model, it could be useful to perform phase field simulations of the complex microsegregation processes as demonstrated for a simple system by [16, 17].

The authors wish to thank K.-H. Warrelmann for the electron probe microanalysis (EPMA) investigations.

References

[1] M. Militzer, E.B. Hawbolt: Austenite grain growth in microalloyed low carbon steels, Grain Growth in Polycrystalline Materials III, TMS (1998) 639.
[2] C. Klinkenberg, K. Hulka, W. Bleck: steel research 75 (2004) 744–752.
[3] W. Yan, Y.Y. Shan, K. Yang: Metall. Mater. Trans. A 38 (2007) 1211–1222.
[4] B. Jansson, M. Schalin, B. Sundman: J. Phase Equilib. 14 (1993) 557–562.
[5] Steel database TCFE3 by Thermo-Calc Software AB, Stockholm/Sweden (http://www.thermocalc.se/) (2005).
[6] N. Saunders, A.P. Miodownik: CALPHAD – Calculation of Phase Diagrams, Pergamon/Elsevier Science Ltd., Oxford/GB (1998).
[7] A. Borgenstamm, A. Engström, L. Höglund, J. Ågren: J. Phase Equilib. 21 (2000) 269–280.
[8] MOB2 mobility database by Thermo-Calc Software AB, Stockholm/Sweden (http://www.thermocalc.se/) (2005).
[9] D. Larouche: CALPHAD 31 (2007) 490–504.
[10] J.-O. Andersson, J. Ågren: J. Appl. Phys 72 (1992) 1350–1355.
[11] S. Crusius, G. Inden, U. Knoop, L. Höglund, J. Ågren: Z. Metallkd. 83 (1992) 673–678.
[12] S. Crusius, L. Höglund, U. Knoop, G. Inden, J. Ågren: Z. Metallkd. 83 (1992) 729–738.
[13] A. Schneider, G. Inden, in: D. Raabe, F. Roters, F. Barlat, L.-Q. Chen (Eds.), Computer Simulation of Diffusion Controlled Phase Transformations, Wiley-VCH, Weinheim (2004) 3–36.
[14] H. Goto, K. Miyazawa, K. Yamaguchi, S. Ogibayashi, K. Tanaka: ISIJ International 34 (1994) 414–419.
[15] J. Miettinen, S. Louhenkilpi, L. Holappa: ISIJ International 36 (1996) Supplement 183–186.
[16] J. Tiaden: J. Crystal Growth 198/199 (1999) 1275–1280.
[17] D. Phelan, M. Reid, R. Dippenaar: Metall. Mater. Trans A 37 (2006) 985–994.

(Received January 8, 2008; accepted April 8, 2008)

Bibliography

DOI 10.3139/146.101689
Int. J. Mat. Res. (formerly Z. Metallkd.)
99 (2008) 6; page 674–679

ISSN 1862-5282

Correspondence address

A. Schneider
Salzgitter Mannesmann Forschung GmbH
Ehinger Straße 200, 47259 Duisburg, Gemany
Tel.: +49 (0)203 999 3194
Fax: +49 (0)203 999 4415
E-mail: a.schneider@du.szmf.de

You will find the article and additional material by entering the document number MK101689 on our website at www.ijmr.de